A Multiband Dual-Antenna System for MIMO Operation in Mobile Terminals

Zhirong An and Mang He

School of Information and Electronics
Beijing Institute of Technology, Beijing, 100081, China
aiyindien@163.com, hemang@bit.edu.cn

Abstract ─ A multiband dual-antenna design for multi-input-multi-output (MIMO) operation in mobile terminals is presented. The proposed dual-antenna system is composed of two symmetric antenna elements, and each of them consists of one driven branch and one parasitic branch. The dual-antenna system uses a simple decoupling structure to reduce the mutual coupling between two antenna elements. The impedance bandwidth with active $|S_{11}|\leq$-6dB covers two frequency bands of 700-960 and 1710-2690 MHz, and the isolation between the two antenna elements is better than 10dB within most of the operating bands. The envelop correlation coefficient, mean effective gain, diversity gain, and channel capacity are calculated exhaustively based on the three-dimensional radiation patterns. The results show that the antenna system has good diversity performance, which makes it suitable for MIMO operation in mobile terminals.

Index Terms ─ Decoupling structure, mobile terminal, multiband antenna, multiple-input-multiple-output operation.

I. INTRODUCTION

MIMO technology can exponentially increase the data transfer rate and spectrum efficiency without any need of increasing the transmission power and bandwidth. At present, MIMO technology has been widely used in base stations, but its application is rather limited in mobile terminals due to crowded space. For antennas in mobile terminals with long term evolution (LTE) functions, the operating bands should cover the LTE 700/2300/2500 (704-787/2300-2400/2500-2690 MHz), UMTS (1920-2170 MHz), GSM 850/900 (824-894/880-960 MHz), DCS (1710-1880 MHz), and PCS (1850-1990 MHz) bands. Meanwhile, in order to ensure that the system has good MIMO performance, high isolation is required between antenna elements. However, because of limited space in mobile terminals, it is difficult to obtain a wide operating band and high isolation simultaneously. Thus, multiband design and inter-elements decoupling are two major challenges for a good MIMO antenna system in mobile terminals.

Recently, several techniques have been proposed to design multiband dual-antenna system for mobile terminals [1]-[5]. In [1], a dual-antenna system consisting of two alphabetic-letter-shaped elements was presented for LTE wireless devices. In [2], a multiband dual-antenna system with high isolation using slotted and protruded ground was presented. A decoupled dual-antenna system with a neutralization line (NL) loaded between the antenna elements was proposed for smartphone applications in [3]. In [4], a dual-antenna system using the decoupling structure with embedded inductors and two crossed NLs was proposed for LTE/ WWAN applications. In [5], a multi-antenna system consisting of inverted-F and open-slot antennas was proposed for LTE MIMO operation. However, there are some deficiencies in previous designs, such as insufficient operating bands [1]-[3], overly complicated structures with folded branch and lumped components [3]-[5], and large sizes [5] etc. In addition, MIMO technology requires all antennas to work simultaneously, but in previous works only the performance of a single antenna was considered, i.e., only one antenna was excited while other antennas were terminated by matched loads. Thus, strictly speaking, this type of antenna system can only be used for the selection-diversity technique, because it allows one antenna to work normally at a time.

In this letter, a design of multiband dual-antenna for mobile terminals is presented. Compared with the previous work, the antenna presented in this paper has a simpler structure and is easy to fabricate under the premise of covering all the required frequency bands. The decoupling structure is theoretically analyzed and the results are in good agreement with simulation and measurement. The simulated and measured results indicate that the proposed antenna design has good MIMO performance.

II. ANTENNA DESIGN

The antenna is modeled by ANSYS HFSS, as shown in Fig. 1 (a). The antenna is placed in an air box with radiation boundary. The size of the box is 350×300×220 mm^3, and the distance between the box boundary and the antenna is quarter of the wavelengths at 700 MHz. The

Submitted On: March 4, 2019
Accepted On: April 6, 2019

antenna is printed on a FR4 substrate with ε_r=4.4 and tanδ=0.02. The size of the substrate is cut to 135×80×0.8 mm^3 to simulate actual mobile terminals of a 6.2-in screen. As in Fig. 1 (b), each antenna element is composed of a dual-line driven branch and a meander-line parasitic branch. The operating band of the longer folded-line in the driven branch covers part of the lower frequencies (800-960 MHz), and the shorter line operates at the higher frequency band (1710-2690 MHz). The parasitic meander-line provides an additional resonant frequency around 750 MHz. Each driven branch is connected to a 50-Ω coaxial line at the feeding point. Fig. 1 (d) shows the decoupling structure which is divided into two parts: the inverted L-shaped strip is designed to reduce the interference of the parasitic branch to the driven branch, and the fence-shaped strips in the middle are used to improve isolation between the two antennas elements. Compared with [4] under the same ground clearance (15mm), this layout makes full use of the limited space, which avoids folding antenna structure in the thickness direction and then reduces the profile of the antenna. Furthermore, the antenna structure is much simpler than those presented in [3]-[5] and is easy to fabricate since no additional lumped element is needed. Through detailed parametric studies, the optimum dimensions of the antenna are listed in Table 1.

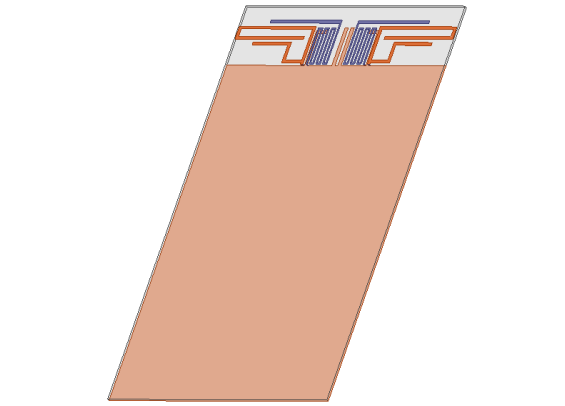

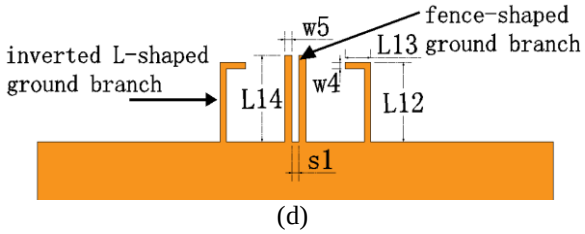

Fig. 1. The proposed dual-antenna system. (a) Simulation model, (b) two antenna elements, (c) sizes of the antenna elements, and (d) decoupling structure.

Table 1: Optimum dimensions of the antenna (Unit: mm)

Parameters	L1	L2	L3	L4	L5	L6
Values	12.9	28	4.4	24	7	6
Parameters	L7	L8	L9	L10	L11	L12
Values	13	12.5	1.7	15	26	12
Parameters	L13	L14	Ls	w1	w2	w3
Values	4	13	0.5	1	0.5	1
Parameters	w4	w5	s1			
Values	1	1.2	1			

A. Antenna structure analysis

MIMO technology requires that all antennas should work simultaneously. Therefore, active *S*-parameters of the proposed antenna are considered, and the active reflection coefficient S_{11a} of a single antenna is related to the passive *S*-parameters S_{11} and S_{12} as follows:

$$S_{11a} = \left(S_{11}a_1 + S_{12}a_2\right)/a_1 = S_{11} + S_{12}\left(a_2/a_1\right), \quad (1)$$

where, a_1 and a_2 are the normalized incident waves at the two ports if we consider the antenna system as a two-port network. The simulated $|S_{11a}|$ of the proposed antenna with and without the parasitic branch are given in Fig. 2. It is clear that the parasitic branch extends the operating bandwidth by adding a resonance at 750 MHz. The current distributions on the two branches are shown in Fig. 3, in which the currents concentrate mainly on the driven branch at 950 MHz and 2.5 GHz while the currents are strong along the parasitic branch at 750 MHz.

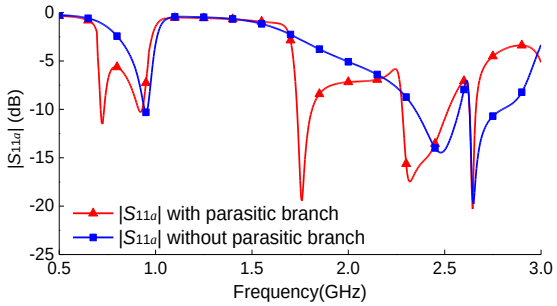

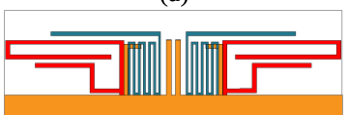

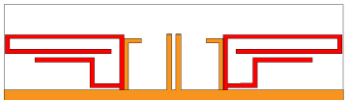

(c)

Fig. 2. The proposed antenna with/without the parasitic branch. (a) Simulated $|S_{11a}|$, (b) antenna with the parasitic meander-line branch, and (c) antenna without the parasitic branch.

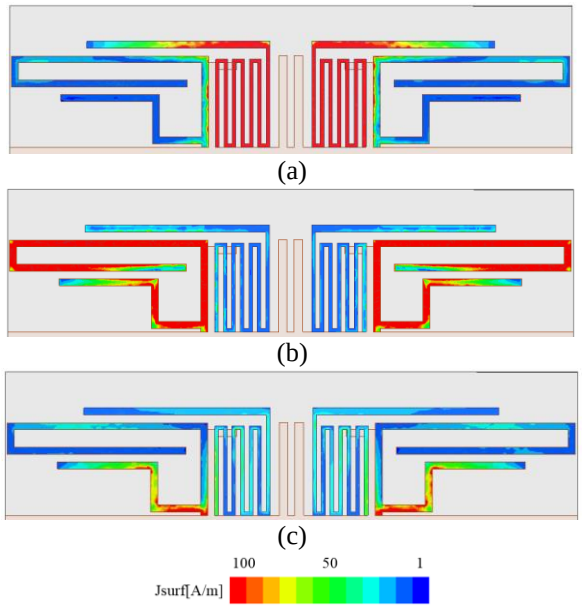

(a)

(b)

(c)

Fig. 3. Current distributions on the proposed dual-antenna system at different frequencies. (a) 750 MHz, (b) 950 MHz, and (c) 2.5 GHz.

B. Design of the decoupling structure

The inverted L-shaped strip in the decoupling structure can decrease the induced current on the parasitic branch at 2.5 GHz as shown in Fig. 4, which improves the impedance matching at higher frequency band as well.

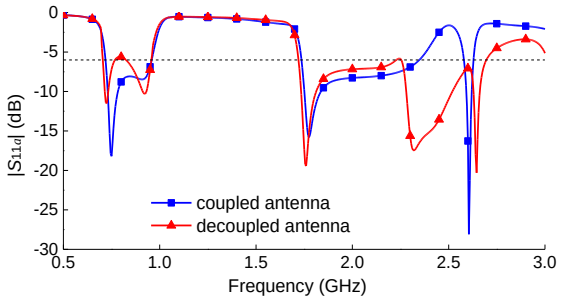

(a)

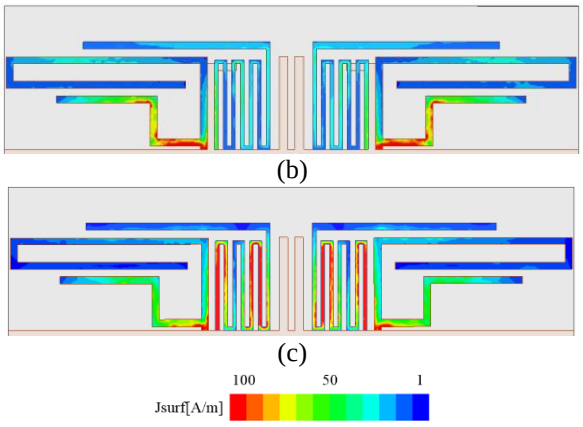

(b)

(c)

Fig. 4. $|S_{11a}|$ and current distributions of the proposed antenna. (a) Simulated $|S_{11a}|$, (b) current distributions on the antenna with the L-shaped strips, and (c) current distributions on the antenna without the L-shaped strips.

The fence-shaped strips in the middle consists of two protruded stubs which are equivalent to two grounded inductors L, and the gap between the two stubs and the gap between the stub and the parasitic branch can be seen as shunt capacitors C and C_0, respectively. Figure 5 presents the equivalent circuit of the structure between the two feeding ports of the antennas.

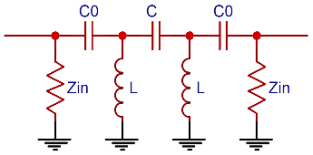

Fig. 5. Equivalent circuit of the fence-shaped strips between two antenna elements.

The corresponding T-matrix can be calculated by cascading the T-matrices of single components:

$$T = T_{Y_{in}} \cdot T_{C_0} \cdot T_L \cdot T_C \cdot T_L \cdot T_{C_0} \cdot T_{Y_{in}}, \tag{2}$$

where, Y_{in} is the admittance of a single antenna, and the involved T-matrices are:

$$\begin{aligned} T_{Y_{in}} &= \begin{bmatrix} 1+Y_{in}/2 & Y_{in}/2 \\ -Y_{in}/2 & 1-Y_{in}/2 \end{bmatrix}, \\ T_{C_0} &= \begin{bmatrix} 1+1/j2\omega C_0 & -1/j2\omega C_0 \\ 1/j2\omega C_0 & 1-1/j2\omega C_0 \end{bmatrix}, \\ T_L &= \begin{bmatrix} 1+1/j2\omega L & 1/j2\omega L \\ -1/j2\omega L & 1-1/j2\omega L \end{bmatrix}, \\ T_C &= \begin{bmatrix} 1+1/j2\omega C & -1/j2\omega C \\ 1/j2\omega C & 1-1/j2\omega C \end{bmatrix}, \end{aligned} \tag{3}$$

in which C_0, C, and L can be calculated by referring to [6]. Then, T_{11} is obtained as:

$$T_{11}=\frac{-\left(\omega C_0-jY_{in}+j\omega^2C_0L+j\omega^2C_0LY_{in}-j\right)\cdot A}{2\omega^5CC_0^2L^2}\ , \quad (4)$$

and

$$A=2\omega^2CL-j\omega C_0-Y_{in}+\omega^2C_0L+2j\omega^3C_0CL +2CL\omega^2Y_{in}+\omega^2C_0LY_{in}-1. \quad (5)$$

The mutual coupling between the two antennas' feeding ports is:

$$S_{21}=1/T_{11}\ . \quad (6)$$

In Fig. 6, it is seen that the fence-shaped strips can effectively reduce the mutual coupling between the antenna elements. In addition, the theoretical curve predicted by equations (2)-(6) is in good agreement with the simulated and measured $|S_{21}|$, which validates the correctness of the theoretical analysis. At the same time, the measured results show that the decoupling structure can achieve 10dB isolation between antennas, which meets the basic requirements of MIMO antenna decoupling. Compared with [2], the proposed decoupling structure is of compact size and is totally arranged within the antenna structure, so any extra space is not needed.

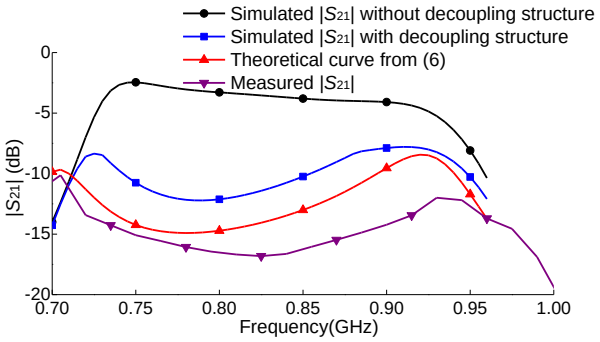

Fig. 6. Theoretical, simulated, and measured $|S_{21}|$ of the proposed antenna.

III. RESULTS AND DISCUSSION

The antenna is fabricated and measured, and the fabricated prototype is shown in Fig. 7. The simulated $|S_{11a}|$ using ANSYS HFSS is given in Fig. 8, which agrees well with the measured data. The measured impedance bandwidth with $|S_{11a}|\leqslant$-6dB is over 700-960 and 1710-2690 MHz, covering all the LTE700/2300/2500, UMTS, GSM850/900, DCS, and PCS bands. As well, the isolation between the two antenna elements is better than 10dB within most of the operating bands.

Figure 9 plots the simulated and measured radiation patterns in three principal planes at two typical operating frequencies in the LTE700/2500 bands. The measured peak gain of the proposed antenna is shown in Fig. 10, which ranges from -1.41 to 1.92 dBi at the lower frequency band and from -0.19 to 5.79 dBi at the higher frequency band. Figure 11 shows the simulation and measured results of radiation pattern null value. The total efficiency of the proposed antenna system is presented in Fig. 12. The total efficiency ranges from 50% to 74.2% at the lower band and from 43.4% to 78.5% at the higher band. Table 2 shows the performance comparison of the proposed antenna with those in existing literature. It is seen that the bandwidth of the proposed antenna covers all the LTE700/2300/2500, UMTS, GSM850/900, DCS, and PCS bands as compared with those in [1]-[3], and the thickness of the design is much smaller than that of the antennas presented in [3]-[5].

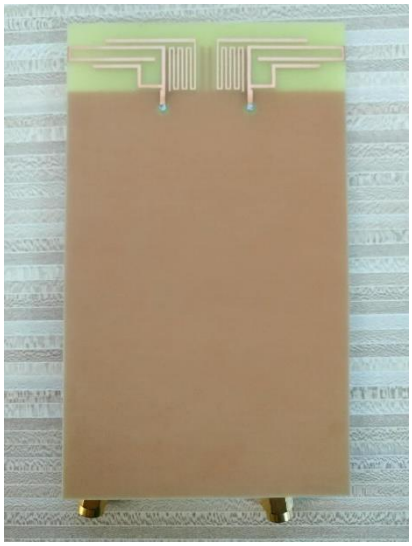

Fig. 7. Fabricated prototype sample.

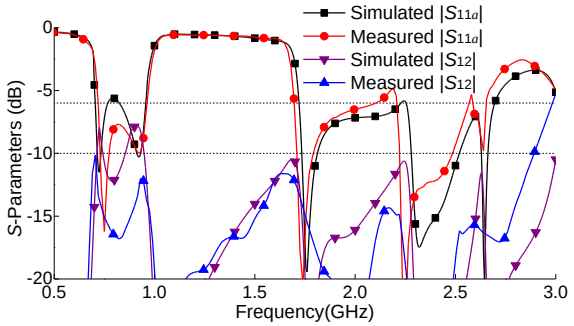

Fig. 8. Simulated and measured *S*-parameters of the proposed antenna.

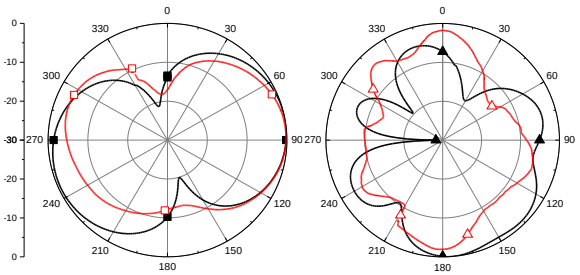

xoy-plane

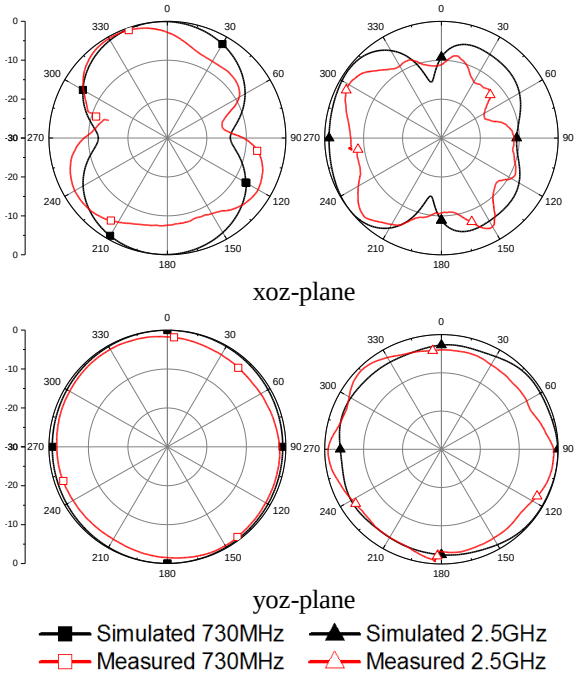

Fig. 9. Simulated and measured radiation patterns.

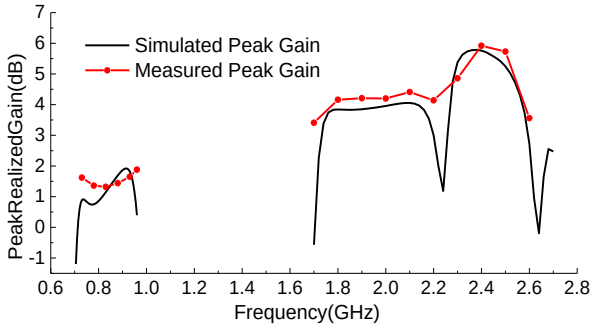

Fig. 10. Peak gain of the proposed antenna.

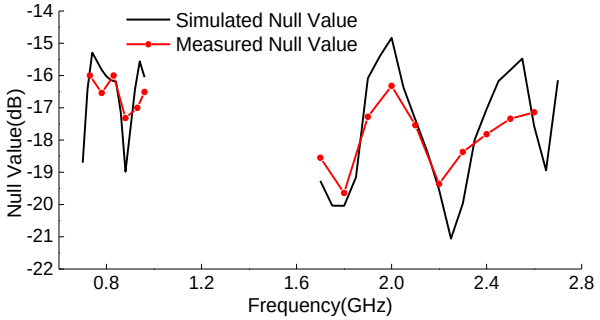

Fig. 11. Null value of the proposed dual-antenna system.

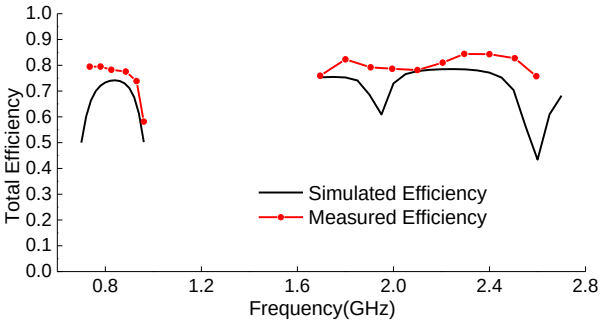

Fig. 12. Total efficiency of the proposed dual-antenna system.

Table 2: Comparison of the proposed antenna with previous works

	Operating Bands (MHz)	Dimension (mm)	Gain (dBi)	Isolation (dB)	Efficiency
Proposed	700-960, 1710-2690	15×80×0.8	-1.41-5.79	10	43.4-78.5
[1]	700-800, 1700-3800	24×70×0.8	1-5	5-15	-
[2]	740-965, 1380-2703	29×60×0.8[a]	0.764-4.505	10	40-67.2
[3]	823-968, 1697-2706	10×70×5	-0.5-3.7	10	40-60
[4]	702-968, 1698-2216, 2264-3000	15×80×5	-1.79-3.75	10	31.86-61.73
[5]	698-960, 1710-2690	8×78×7	-	10	45-83

[a]The area occupied by the slotted ground is calculated.

In order to investigate the diversity performance of the proposed antenna system, some critical parameters [7]-[10] are calculated:

$$\rho_e = \frac{\left|\iint_{4\pi}\left[\vec{F}_1(\theta,\phi)\bullet\vec{F}_2(\theta,\phi)\right]d\Omega\right|^2}{\iint_{4\pi}\left|\vec{F}_1(\theta,\phi)\right|^2 d\Omega \iint_{4\pi}\left|\vec{F}_2(\theta,\phi)\right|^2 d\Omega}, \tag{7}$$

$$\text{MEG}=\int_0^{2\pi}\int_0^{\pi}\left(\frac{\text{XPR}}{1+\text{XPR}}G_\theta(\theta,\phi)P_\theta(\theta,\phi) + \frac{1}{1+\text{XPR}}G_\phi(\theta,\phi)P_\phi(\theta,\phi)\right)\sin\theta d\theta d\phi, \tag{8}$$

$$\text{DG} = \left[\frac{\gamma_C}{\Gamma_C}-\frac{\gamma_1}{\Gamma_1}\right]_{P(\gamma_C<\gamma_S/\Gamma)}, \tag{9}$$

$$C = E\left\{\log_2\left[\det\left(I+\frac{SNR}{n_T}HH^H\right)\right]\right\}, \tag{10}$$

and the results are given in Fig. 13. It is observed that the envelope correlation coefficient (ECC) is less than

0.16 within the entire frequency bands, and comparable average received power (|MEG1/MEG2| <3dB) and high diversity gain (DG > 9.6 dB) at 1% of the cumulative distributed functions are obtained. Figure 14 provides the channel capacity of the proposed antenna design. It is seen that the channel capacity is more than 9.5 bps/Hz with 20dB SNR, which is much improved compared with the SISO antenna.

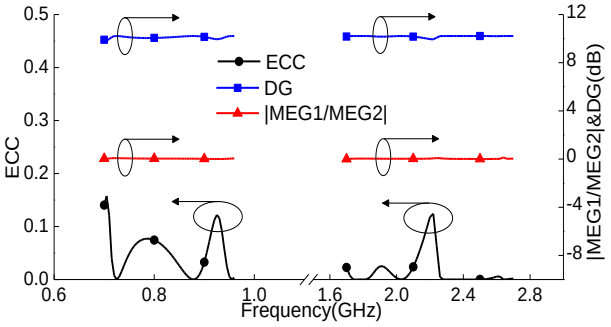

Fig. 13. Diversity performance of the proposed antenna.

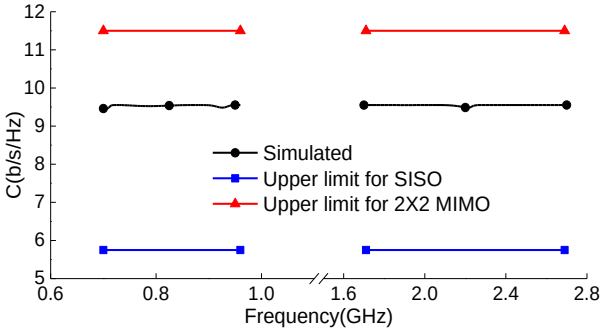

Fig. 14. Simulated channel capacity of the proposed antenna.

IV. CONCLUSION

In this letter, a multiband dual-antenna design for MIMO operation in mobile terminals is presented. The measured impedance bandwidth with $|S_{11a}|\leqslant$-6dB is over 700-960 and 1710-2690 MHz, covering all the LTE700/2300/2500, UMTS, GSM850/900, DCS, and PCS bands. The isolation between the two antenna elements is better than 10dB within most of the operating bands. The simulated and measured results show that the proposed antenna design has good diversity performance and high channel capacity, which makes it suitable for MIMO operation in mobile terminals.

REFERENCES

[1] F. Ahmed, M. H. M. Chowdhury, and A. M. A. Rahman, "A multiband MIMO antenna for future generation handset applications," *2017 International Conference on Electrical, Computer and Communication Engineering (ECCE)*, Cox's Bazar, pp. 91-94, 2017.

[2] J. Dong, X. Yu, and L. Deng, "A decoupled multiband dual-antenna system for WWAN/LTE smartphone applications," *IEEE Antennas and Wireless Propagation Letters*, vol. 16, pp. 1528-1532, 2017.

[3] Y. L. Ban, C. Li, C. Y. D. Sim, G. Wu, and K. L. Wong, "4G/5G multiple antennas for future multimode smartphone applications," in *IEEE Access*, vol. 4, pp. 2981-2988, 2016.

[4] S. Wang and Z. Du, "Decoupled dual-antenna system using crossed neutralization lines for LTE/WWAN smartphone applications," in *IEEE Antennas and Wireless Propagation Letters*, vol. 14, pp. 523-526, 2015.

[5] I. R. R. Barani and K. Wong, "Integrated inverted-F and open-slot antennas in the metal-framed smartphone for 2×2 LTE LB and 4×4 LTE M/HB MIMO operations," in *IEEE Transactions on Antennas and Propagation*, vol. 66, no. 10, pp. 5004-5012, Oct. 2018.

[6] K. Sarabandi and N. Behdad, "A frequency selective surface with miniaturized elements," in *IEEE Transactions on Antennas and Propagation*, vol. 55, no. 5, pp. 1239-1245, May 2007.

[7] S. Blanch, J. Romeu, and I. Corbella, "Exact representation of antenna system diversity performance from input parameter description," in *Electronics Letters*, vol. 39, no. 9, pp. 705-707, 1 May 2003.

[8] Y. Li, B. Yu, H. Shen, L. Zhu, and G. Yang, "An 8-port planar UWB MIMO antenna for future 5G micro wireless access point applications," *2017 International Applied Computational Electromagnetics Society Symposium (ACES)*, Suzhou, pp. 1-2, 2017.

[9] T. Taga, "Analysis for mean effective gain of mobile antennas in land mobile radio environments," in *IEEE Transactions on Vehicular Technology*, vol. 39, no. 2, pp. 117-131, May 1990.

[10] A. Diallo, C. Luxey, P. Le Thuc, R. Staraj, and G. Kossiavas, "Diversity performance of multi-antenna systems for UMTS cellular phones in different propagation environments," *International Journal of Antennas & Propagation*, vol. 2008 (1687-5869), pp. 264-276, 2008.